Analytical Biochemistry 385 (2009) 234–241

Contents lists available at ScienceDirect

Analytical Biochemistry

journal homepage: www.elsevier.com/locate/yabio

Whole serum BSA antibody screening using a label-free biophotonic nanoparticle array

Rouslan V. Olkhov, Jeremy D. Fowke, Andrew M. Shaw *

School of Biosciences, University of Exeter, Geoffrey Pope Building, Stocker Road, Exeter EX4 4QD, UK

ARTICLE INFO

Article history:
Received 6 August 2008
Available online 5 November 2008

Keywords:
Plasmon resonance
Array screening
Label-free
Protein–protein interactions

ABSTRACT

Bovine serum albumin antibodies (aBSA) have been screened from whole leporine anti serum on a biophotonic array. The array was initially printed with seed gold nanoparticles into a 96-spot configuration, and 130-nm gold nanoparticles were synthesised in situ on the surface of each spot. The gold nanoparticle surface was then functionalized with the proteins bovine serum albumin (BSA), fibrinogen, and immunoglobulin G (IgG) and with the amino acid glycine. The concentration of aBSA in the whole serum was determined using a kinetic analysis of the time-dependent light scattering from the nanoparticles. The aBSA–BSA kinetic parameters derived from the array are $k_a = (1.3 \pm 0.3) \times 10^5\ M^{-1}\ s^{-1}$, $k_d = (4 \pm 2) \times 10^{-4}\ s^{-1}$, and $K_D = 3$ nM, which compare favorably with those from continuous gold surfaces. The ultimate sensitivity of the array reader to the bulk refractive index (*RI*) is 1×10^{-4} refractive index units (RIU), corresponding to 1 μg ml^{-1} for aBSA. The nanoparticles appear to be more sensitive than the continuous gold surface to the aBSA binding event from whole serum, and this is interpreted in terms of the difference in *RI* contrast in the plasmon fields.

High-throughput screening of DNA and proteins on array chip platforms using labeled technologies is now being used extensively in the field of systems biology. Protein chip arrays in particular have been used to profile the transcriptome of organisms such as profiling the transcriptome of whole organisms, including cancer cells [1,2] and the human transcriptome [3]. The expectation is that analysis of the expression patterns of a whole organism will lead to an understanding of the complexity of the system, although this is only the beginning of the challenge given that the role of metabolites and signaling sugars is not yet included in the current array approaches [4]. However, all of the current applications use labeled detection, usually fluorescence, to detect the presence or absence of a protein. Fluorescence is intrinsically vulnerable to quenching, and the data can be only semiquantitative at best. Given the overhead time required to prepare the arrays, a simple presence or absence of a protein or a semiquantitative result is limiting, whereas a label-free technology would ideally provide kinetic information and absolute quantitative concentration levels of proteins generating information-rich data from the array.

The current lead technology for label-free screening is based on the optical properties of the gold plasmon either on a continuous surface, surface plasmon resonance (SPR),[1] or as a nanoparticle, localized particle plasmon [5]. The majority of the conventional SPR platforms such as Biacore provide a two-channel analysis allowing the interrogation of single protein–protein interactions [6] from which kinetic parameters have been derived. The extension to multiplex systems is also now beginning with instruments such as the Biacore Flexchip, SPRi-Plex, GWC SPRimagerII, and Graffinity for label-free protein expression analysis [7–9].

An advantage of gold nanoparticle structures over continuous gold surface platforms for biosensing applications is the potential to tailor the optical properties of the nanoparticle for each specific assay [10]. Single nanoparticles have been suggested as possible biosensors [11], and enhancement sensitivity to the biological processes has been achieved by control of the geometry such as nanopin optical resonators [12]. Optimization of the particle shape allows the scattering properties, maximum scattering wavelength, and (important for screening complex fluids such as blood serum) the penetration depth, d_p, of the plasmon field into the surrounding medium to be tailored. The optical properties of the particle plasmon change in response to the biochemical binding event in the plasmon field of the particle that typically penetrates $d_p \sim 20$ nm.

* Corresponding author.
E-mail address: andrew.m.shaw@exeter.ac.uk (A.M. Shaw).

[1] *Abbreviations used:* SPR, surface plasmon resonance; BSA, bovine serum albumin; IgG, immunoglobulin G; EDC, *N*-(3-dimethylaminopropyl)-*N*′-ethylcarbodiimide hydrochloride; NHS, *N*-hydroxysuccinimide; $HAuCl_4$, gold(III) chloride trihydrate; $AgNO_3$, silver nitrate; CTAB, cetyl–trimethyl–ammonium bromide; $C_6H_5Na_3O_7$, sodium citrate; $NaBH_4$, sodium borohydride; $C_6H_8O_6$, (l+) ascorbic acid; DTSP, dithiobis-succinimidyl propionate; SEM, scanning electron microscope; *RIS*, refractive index sensitivity; DMSO, dimethyl sulfoxide; PBS, phosphate-buffered saline; aBSA, BSA antibodies; *RI*, refractive index; RIU, refractive index units; Re, Reynolds number; PSA, prostate-specific antigen.

0003-2697/$ - see front matter © 2008 Elsevier Inc. All rights reserved.
doi:10.1016/j.ab.2008.10.042

This may be compared with $d_p \sim 300$ nm for the continuous gold surface in SPR instruments [13–15]. Hence, the nanoparticles are less susceptible to the "biological noise" in the complex fluid that is present in more than 90% of the plasmon field of a continuous surface. Taking this further, electron beam lithography allows gold particles to be designed and engineered in both size and shape and to be arranged in regular or random configurations to maximize the sensitivity of the particle plasmon to the binding event [16,17].

Control and optimization of the nanoparticle surface for label-free detection determines the optical sensitivity of the technique, but the biological specificity requires careful design of the biological assay printed onto each spot of the array. Kinetic analysis of immunoassays for the specific detection of analytes [18] enables the concentration of the target species in solution to be determined [19]. The accuracy of the concentration determination, especially in complex fluids such as sera, depends on competing processes such as nonspecific binding of blood proteins to the bioassay.

Here we present a microarray biosensor platform based on optical scattering properties of gold nanoparticles that have been synthesized in situ on the substrate surface. The array is then functionalized with three proteins—bovine serum albumin (BSA), immunoglobulin G (IgG), and fibrinogen—as well as the amino acid glycine. The whole antiserum for BSA is analyzed using a simple array reader. We previously presented the preliminary results from the array reader [20] from which it is possible to derive kinetic parameters and, hence, analyte concentrations. In the current article, we compare the results from the array reader with those from the Nomadics SensiQ continuous gold SPR platform to establish the sensitivity of the nanoparticle arrays in the complex whole blood sera and to investigate the role of control spots in the kinetic analysis of the data.

Materials and methods

The study of the label-free protein–protein interactions was performed using our custom-fabricated array reader, which interrogates an array printed on a glass slide in a near-field illumination configuration. Light scattered from the array is collected normal to the slide surface, and the variation of the scattered light intensity is monitored in real time. Each element of the array is functionalized with a protein, and the change in the scattered light intensity allows the kinetics of the protein–protein interaction to be determined. The array reader flow cell must allow concentration-limited kinetics to ensure that the rate of adsorption is limited by the concentration of the analyte in solution and not by the diffusion and flow characteristics. A kinetic analysis of the time-varying scattered light intensity for each bioassay is then performed, and from this the concentration of the antibodies in the serum may be determined.

The array reader

The label-free array reader design was discussed briefly elsewhere [20] but is presented in detail here. The array reader consists of near-field illumination configuration using a Dove prism that is integral to the flow cell (Fig. 1). Radiation from continuous wave laser diode (532 nm, 5 mW, Scitec Instruments) is expanded in a Keplerian telescope to give a beam of 4 mm diameter to probe the array of 2.7 × 3.3 mm physical dimensions. Radiation scattered normal to the surface of the array is collected by an objective lens (35 mm/f3.5, Pentax) adapted for macroimaging and detected using a digital video camera (640 × 480 pixels, monochrome, Luminera). Images of the array surface are taken at 15 Hz and transferred to the computer, where they are averaged over a period of 1 s (15 frames). Image analysis software searches for the array

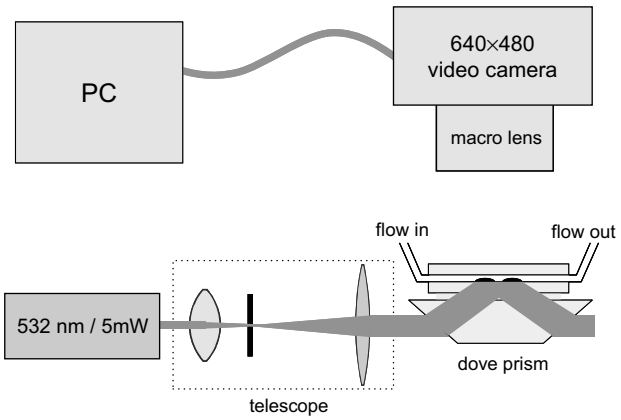

Fig. 1. Schematic diagram of the sensor array reader.

spots within the regular pattern of the array mask, which is then refined to the position of the actual spots. Each array spot is typically 150 μm diameter, corresponding to 128 pixels in the acquired image. The averaged intensity within each area gives the brightness of the array spot that is followed in real time. The laser intensity fluctuations across the surface of the array are normalized to the initial brightness.

The performance of the array reader is compared with a commercial SensiQ SPR instrument from ICX Nomadics. The instrument is an integral chip containing the light source, the detector, and the two-channel, carboxyl-functionalized sensor surface. Proteins were immobilized on the carboxyl surface by activation of the carboxyl groups with *N*-(3-dimethylaminopropyl)-*N*′-ethylcarbodiimide hydrochloride (EDC) and *N*-hydroxysuccinimide (NHS). The protein is immobilized through any primary amine on its surface, which displaces the NHS leaving group, forming a peptide bond—a conventional EDC/NHS coupling chemistry [21]. There is no control over the orientation of the protein on the surface, but statistically all possible surfaces—including the epitope for the antibody—are presented.

Chemicals

Gold(III) chloride trihydrate ($HAuCl_4 \cdot 3H_2O$, 99.9%), silver nitrate ($AgNO_3$, 99%), cetyl–trimethyl–ammonium bromide (CTAB, 95%), sodium citrate ($C_6H_5Na_3O_7 \cdot 2H_2O$, 99.9%), BSA (98%), fibrinogen (60%), murine IgG (80%), delipidized whole antiserum anti-BSA (developed in rabbit, 3.7 mg/ml BSA antibody, 60 mg/ml other serum proteins, product no. B1520), EDC (98%), and NHS (98%) were obtained from Sigma–Aldrich. Glycine (analytical grade) was supplied by Fisher Scientific. Sodium borohydride ($NaBH_4$, 98%) was supplied by Lancaster. (L+) Ascorbic acid ($C_6H_8O_6$, 99%) was obtained from Acros. Dithiobis-succinimidyl propionate (DTSP, 97%) was supplied by Fluka. Throughout the experiments, 18 kΩ deionized water was used as a solvent when required.

Photonic surface preparation

The in situ synthesis of the gold nanoparticles forming the photonic surface allows the physical dimensions and the orientation of the array to be established easily. The array preparation sequence is as follows: (i) the seed nanoparticles are printed from a colloid using an inkjet printer; (ii) the slides are removed from the printer and placed into the growth solution; (iii) the slides are washed; and (iv) the slides are returned to the printer to print the array assays. The seed particles are spherical gold nanoparticles with a diameter in the range of 3 to 4 nm and are prepared using a rapid

sodium borohydride reduction of Au(III) to Au(0) and then stabilized with a citrate surface ligand. Then 0.6 ml of ice-cold 0.1 M $NaBH_4$ solution was rapidly added to the 20-ml solution containing 3×10^{-4} M $HAuCl_4$ and 3×10^{-4} M sodium citrate, stirring quickly. The resulting gold colloid was left to mature for 2 to 3 h before the printing step.

The seed nanoparticles were printed in 12×8 rectangular arrays on an uncoated 25×25-mm square glass slide using an inkjet printer (Arrayjet Aj100). The seed colloid is mixed with glycerol in a 3:1 ratio to ensure the correct viscosity for the printing buffer for well-formed spots during the inkjet printing step. The printed slides were dried in air (50 °C, 20 min), and excess glycerol along with particles not adhering to the slide surface were washed off with water; after rinsing the slides were visually transparent.

The gold nanoparticles responsible for the photonic properties of the sensor array are synthesized on the glass slide surface using a seed growth-mediated wet chemistry similar to the solution chemistry proven for the synthesis of rod-shaped particles [22,23]. The objective is to extend the particles, ideally producing one target shape particle with optimized photonic properties. The growth solution contains 0.1 M CTAB, 2×10^{-4} M $HAuCl_4$, 2×10^{-6} M $AgNO_3$, and 4×10^{-4} M ascorbic acid. The slides are completely immersed in the growth solution for 20 min at an approximate temperature of 28 °C. After the surface synthesis, the arrays are clearly visible on the surface of the glass slide with a characteristic reddish-brown color. The growth phase requires the surfaces to be stabilized by the surfactant CTAB, which remains over the surface of the particles and the slide after the synthesis is complete. The surface of the particles needs to be clean and free from the CTAB to ensure accurate biofunctionalization, and the CTAB is removed through extensive washing cycles in water. The resulting nanoparticles have been imaged by a scanning electron microscope (SEM) (Fig. 2) and show a truncated polyhedral shape with an average diameter of 130 ± 6 nm (mean ± SD).

The final array is shown in Fig. 3A under near-field illumination in the array reader. Although the regular pattern of spots covered with gold nanoparticles is successfully produced, the brightness of the individual spots is not uniform across the area of the spot, with marked enhanced brightness around the perimeter of each spot. This is thought to reflect the concentration profile of the seed particles left in the drying pattern on the surface of the substrate. To compensate for the nonuniformity of the spot, some image filters have been developed to maximize the refractive index sensitivity (*RIS*), removing pixels where there is no brightness change. This reduces the number of working pixels under each spot from approximately 128 to 100.

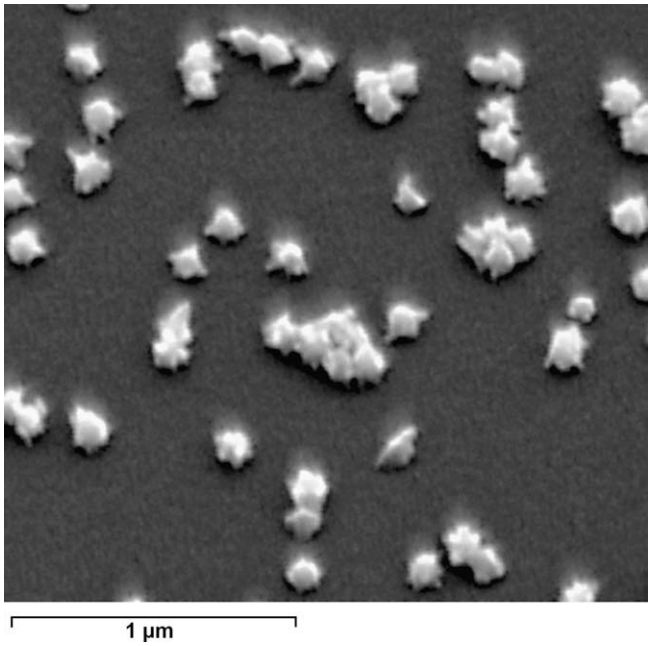

Fig. 2. SEM image of the nanoparticles grown from gold seed particles deposited on silica substrate. Coverage = 14 ± 2%; size = 130 ± 6 nm.

Bioarray printing

The nanofabricated photonic surface on each spot of the array may then be functionalized with the proteins for the assays, printing control spots nearby. The entire slide is immersed in a solution of DTSP (1 mg ml^{-1} in 1:1 [v/v] isopropanol/dimethyl sulfoxide [DMSO]) [21], which contains a dithiol group that dissociates at the gold surface specifically forming the stable S-Au and a highly reactive succinimidyl ester. Attack by primary amine groups on the outer surface of the target protein results in peptide coupling to the sensor surface, which is stable in physiological conditions and at moderately low and high pH levels. Slides were immersed in the DTSP solution at room temperature for 15 min, washed with isopropanol, and dried. This completes the first step.

The second step requires the proteins to be printed to each array spot. This must be performed rapidly because the DTSP succinimidyl ester has a hydrolysis half-life of approximately 20 min [21], which restricts the protein number density on the surface. Concentrated protein solutions (1 mg/ml BSA, 0.6 mg/ml fibrinogen, 0.06 mg/ml IgG, in phosphate-buffered saline [PBS]) and glycine (20 mg/ml in PBS) are printed in the pattern shown in Fig. 3B, with a number of repetitions of each assay distributed across the array to improve statistical significance. The printed drops have a volume of approximately 0.3 nl per spot; they are incubated for 40 min to allow the coupling reaction to be completed. The excess solution is washed with water, and the slides are then stored at 5 °C.

The array design allows comparison of specific and nonspecific BSA antibodies (aBSA)–BSA binding using fibrinogen, IgG, or glycine spots as a control. The responses from each spot with identical assays are averaged to provide the kinetic trace for the binding of the antiserum to the target protein on the array surface.

Results

The sensitivity of the array spots to both bulk and local refractive index (*RI*) changes are important parameters in the design of the array reader. The sensitivity to bulk *RI* is assessed by changing the composition of a solvent above the array with binary mixtures of isopropyl alcohol and water; each mixture has a tabulated *RI* value [24]. The sensitivity of the array prior to functionalization with the adsorbed proteins is assessed by monitoring the change in the scattered intensity as a function of bulk *RI* composition. A change in the bulk index from 1% isopropanol in water to pure water is shown in Fig. 4A. The *RI* of the binary mixture from pure water to pure isopropanol varies over the range of 1.333 to 1.377 at 20 °C and standard pressure. The change in scattered brightness with *RI* is shown in Fig. 4B, illustrating a linear correlation with correlation coefficient $r^2 = 0.9992$ and $\chi^2 = 5.796 \times 10^{-7}$. The gradient of the linear fit is 174 ± 2% RIU^{-1} for the data presented in Fig. 4B. This gradient is a measure of relative sensitivity of the manufactured photonic surface to the bulk *RI* and is used to characterize the sensitivity of the different nanoparticles synthesized under different growth conditions. The sensitivity for all surfaces fabricated during these experiments falls in the range of 150 to

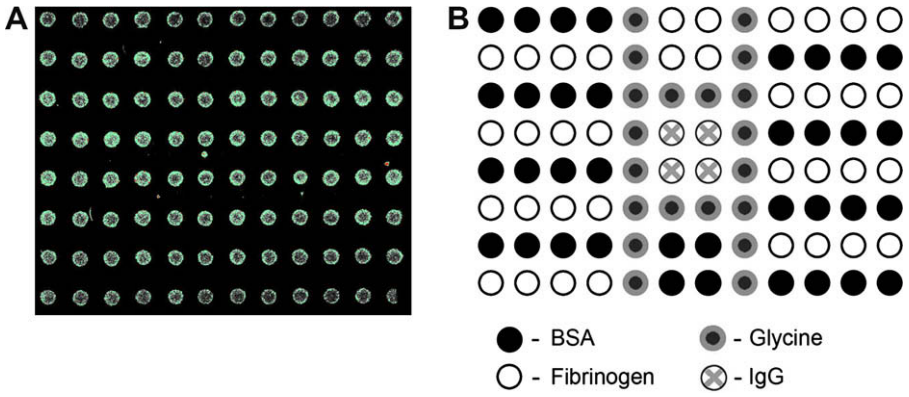

Fig. 3. Array. (A) Image in the array reader. (B) Key to the array assay locations.

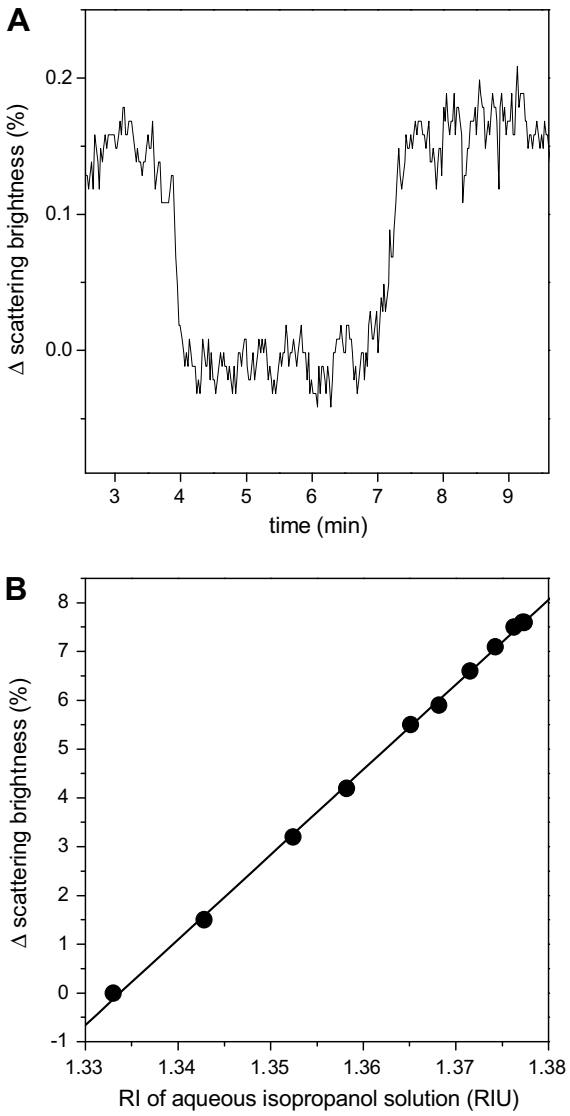

Fig. 4. (A) Sensitivity to the change of the bulk *RI* on switch of the analyte solution from 1% aqueous isopropanol to water. Estimated $RIS = 1.5 \pm 10^{-4}$ RIU. (B) Linearity of the light scattering response to the change in the bulk *RI* of the analyte solution. $r^2 = 0.9992$; $\chi^2 = 5.796 \times 10^{-7}$.

500% RIU^{-1}. The sensitivity of the surface is derived from the optical properties of the nanoparticles, their geometrical parameters [25], seed particle surface density, and surface synthesis conditions [20]; however, similar sensitivities and properties are observed from consistent operating procedures.

The effect of bulk *RI* on the light scattering behavior can be used to describe the smallest detectable change of bulk *RI;* hence, the absolute *RIS* of the sensor may be written as

$$RIS = \sqrt{2}\sigma_1 \left| \frac{RI_1 - RI_2}{I_1 - I_2} \right| \quad (1)$$

where mean *I* is scattered light intensity and σ_I is its standard deviation. Subscripts 1 and 2 would correspond to analytes with different bulk *RI* values. Fig. 4B shows how the light scattering intensity follows the analyte *RI* change. Typically, the manufactured sensor arrays demonstrated a mean *RIS* of approximately 5×10^{-4} RIU, but the spot-to-spot variability was far from ideal and the *RIS* of spots on the same sensor ranged from 1.5×10^{-4} to 8×10^{-4} RIU for each spot.

The array reader performance and sensitivity depend on the response of the surface to proteins binding to the gold surface or formally a change in the polarizability of the medium within the plasmon field. This may be measured by the response of the spot to protein binding, the rate of adsorption, and the total change in *RI* for a monolayer coverage. The smallest detectable change and the rate of adsorption to the surface are important characteristics both of the surface–protein interactions and the system fluidic regime. It is essential that the fluidic parameters are not limiting the kinetics of the protein–protein interactions and that the flow cell parameters have been optimized. The fluidic parameters for two flow cell designs for the array reader are compared with the flow cell characteristics for the SensiQ SPR instrument in Table 1. Flow cell A has a large volume and a low Reynolds number (Re), requiring a large sample and slow transport properties to the surface. Flow cell B and the SensiQ flow cells have similar volumes and higher Reynolds numbers, requiring much smaller samples and better transport properties. The rate constant for the adsorption of aBSA to a BSA-functionalized surface is shown in Fig. 4A as a function of the flow rate through the SensiQ flow plasmon chip. The observed antibody–antigen binding rate increases with increasing flow rates until a concentration-limited rate is observed at 30 μl min^{-1}, (Fig. 5A). At this flow rate, the association rate con-

Table 1
Microfluidic parameters for the SensiQ and array reader flow cells.

	V (nl)	Hydraulic diameter (μm)	Linear flow velocity (mm s^{-1})	Reynolds number
Array cell A	90,000	3000	0.47	3
Array cell B	1500	30	29	300
SensiQ	85	28	37	200

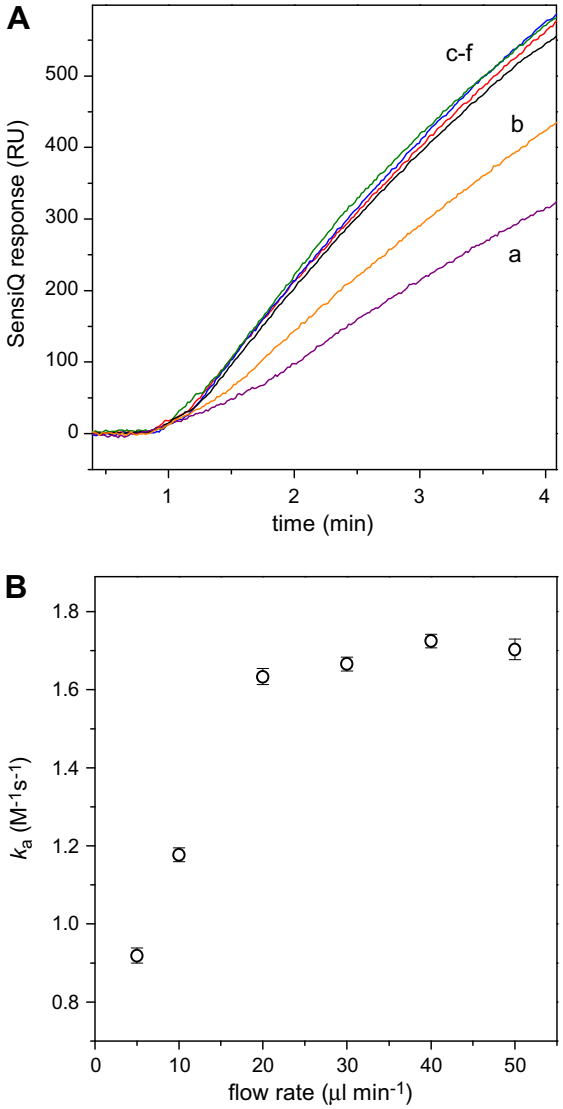

Fig. 5. Effect of the analyte flow rate used in the SensiQ-based experiments on the observed BSA antibody–antigen association rate. (A) Transient response curves corresponding to 5-µl/min (a), 10-µl/min (b), 20-µl/min (c), 30-µl/min (d), 40-µl/min (e), and 50-µl/min (f) flow rates of approximately 14 nM anti-BSA analyte solution. (B) Association rate constants derived from the curves shown in panel A.

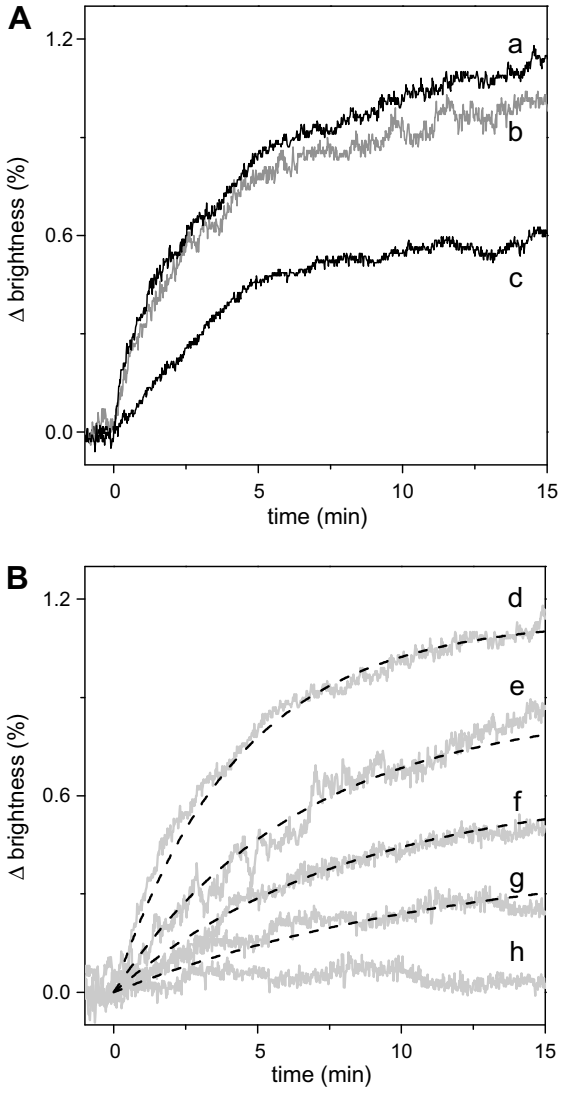

Fig. 6. Dependence of the transient scattering signal corresponding to the BSA antibody–antigen binding on the chosen reference and the concentration of a BSA in analyte solution. (A) Fixed [aBSA] = 28 nM with varying reference: (a) glycine; (b) IgG; (c) fibrinogen. (B) Glycine reference with varying [aBSA]: (d) 28 nM; (e) 18 nM; (f) 14 nM; (g) 9 nM; (h) control buffer injection. Dashed curves are simulations based on $k_a = 1.3 \times 10^5\ M^{-1}\ s^{-1}$.

stant is $(1.7 \pm 0.2) \times 10^5\ M^{-1}\ s^{-1}$ (mean ± 2SD) (Fig. 5B). The SensiQ and array reader SPR platforms (with flow cell B) produce comparable rate constants for the BSA–aBSA adsorption, establishing confidence in the performance of the array reader.

Having established a concentration-limited flow regime, the array printed according to the key in Fig. 3B was analyzed. The IgG, glycine, and fibrinogen all are expected to show nonspecific binding when the BSA antiserum is introduced to the array. Therefore, each of the other protein-functionalized spots could act as a nonspecific binding control spot for the aBSA binding to BSA. Binding of aBSA to BSA using IgG, fibrinogen, and glycine as control surfaces is shown in Fig. 6A, where the largest surface coverage for binding can be seen in channels a and b, that is, the glycine- and IgG-functionalized spots. Using glycine as the reference, the response of the nanofabricated surfaces to varying concentrations of aBSA was measured and is presented in Fig. 6B. Confidence in the correct kinetic response of the surface requires the adsorption rate for aBSA–BSA to be the same as that observed for the continuous gold surface platforms. The detailed association rate for aBSA–BSA is shown in Fig. 7, and the dissociation rate may be observed following the buffer change. The response of each spot may be calibrated for *RI* change based on the response of the surface to the bulk *RI* changes of solvent, and this is plotted on the right-hand axis of Fig. 7; binding 9.5 nM aBSA to the BSA assay spots using the glycine channel as a control produces a $\triangle RI_{bulk} = (4.6 \pm 0.1) \times 10^{-3}$ after approximately 18 min of deposition time.

Discussion

The response of the nanofabricated surface requires the nanoparticle scattering intensity to change on binding the target species. Ideally, this change should be linear, and within the flow cell of the instrument this should lead to concentration-limited kinetics. The results from the array reader have been compared at each stage with the SensiQ continuous gold surface SPR platform and, therefore, are comparable with all SPR surfaces. The variation in scattered intensity depends both on the choice of wavelength and on maintaining constant laser illumination over the surface

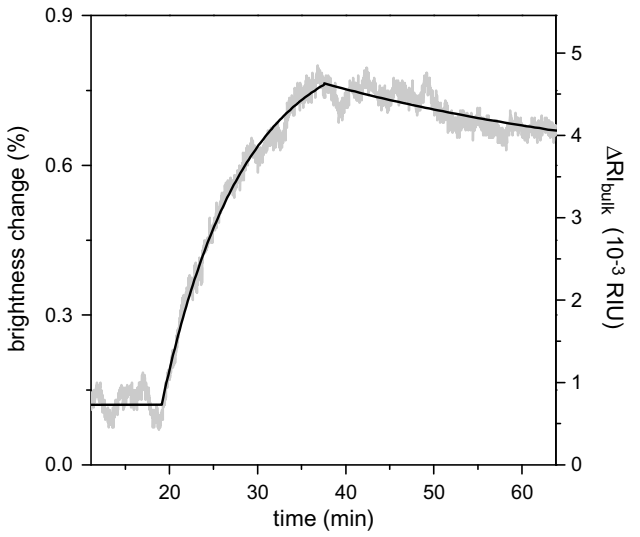

Fig. 7. Transient scattering signal observed on sensor array exposure to the 9.5-nM BSA antiserum solution using a glycine reference spot. Solid black curves correspond to the best fit curves from Eq. (4): $k_a = (1.4 \pm 0.2) \times 10^5\ M^{-1}\ s^{-1}$ and $k_d = (4 \pm 2) \times 10^{-4}\ s^{-1}$.

of the array. The temporal laser power fluctuations are a limit to the performance of the current instrument. A significant advantage of the array configuration is the availability of control spots to control for a number of instrumental effects, most of which are removed by simply averaging the assay response over a number of assay spots. Both the careful use of control spots and the assay averaging increase the signal-to-noise ratio, sensitivity, and confidence level in the performance of the array reader.

For the continuous surface and particle plasmon sensors, the arrival of the protein in the plasmon field changes the plasmon, and this is usually monitored as a change in maximum excitation angle or scattering intensity. Importantly, the plasmon characteristics will change irrespective of whether the proteins bind specifically or nonspecifically to the functionalized surface. Successful binding to the biospecific surface is the source of the signal; nonspecific binding or protein presence in the plasmon field, but not at the surface, is a source of biological noise to the detection event. Determination of the concentration of the target analyte in solution requires a kinetic analysis of the assay biospecific binding event; an array spot with constant protein surface coverage and a known association rate constant will cause a change in the scattering intensity from which the concentration may be derived.

A model describing the kinetic response for aBSA binding to the BSA-functionalized array assay spot may be expressed as follows:

$$\frac{d\vartheta}{dt} = k_a[\mathrm{aBSA}](\vartheta_{m,\mathrm{aBSA}} - \vartheta_{\mathrm{aBSA}}) - k_d\vartheta_{\mathrm{aBSA}} + \sum_i {}^n k_{a,i}[\mathrm{prot}_i](\vartheta_{m,i} - \vartheta_i) - \sum_i {}^n k_{d,i}\vartheta_i. \quad (2)$$

The first three terms in Eq. (2) are the conventional Langmuirian adsorption isotherm with surface coverage ϑ, k_a is the adsorption rate constant, and k_d is the desorption rate constant. The maximum coverage for the BSA on the surface is given by ϑ_m, which is competitive with all other proteins also landing on the surface. $\vartheta_{m,i}$ is the coverage for each protein$_i$, where i is the running index relating to all other proteins in the antiserum and $\sum \vartheta_{m,i} = 1$ for a complete monolayer. The summation term in Eq. (2) is a sum over all possible proteins [prot$_i$] in the antiserum binding to the surface with a similar Langmuirian adsorption isotherm. Each process is modeled by an adsorption rate constant ${}^n k_{a,i}$, a desorption rate constant ${}^n k_{d,i}$, and a surface coverage $\vartheta_{m,i}$ and ϑ_i.

The data do not allow the complete separation of these processes, but a compensation for nonspecific binding is possible by subtraction of the temporal response from a control spot on the array. Subtracting the control trace gives

$$\frac{d\vartheta}{dt}(\mathrm{BSA}) - \frac{d\vartheta}{dt}(\mathrm{control}) = \frac{d\Delta\vartheta}{dt} = k_a[\mathrm{aBSA}](\vartheta_{m,\mathrm{aBSA}} - \vartheta_{\mathrm{aBSA}}) - k_d\vartheta_{\mathrm{aBSA}}. \quad (3)$$

There are some hidden assumptions in this procedure, principally that the ${}^n k_a$ and ${}^n k_d$ constants are the same for interactions between blood proteins and differently functionalized spot surfaces. Eq. (3) may be integrated analytically to give

$$\Delta\vartheta(t) = \vartheta_m k_a[\mathrm{aBSA}]\frac{1 - \exp(-(k_a[\mathrm{aBSA}] + k_d)t)}{k_a[\mathrm{aBSA}] + k_d}, \quad (4)$$

where ϑ_m, k_a, and k_d are fitting parameters, although k_d is too small to be determined accurately during the adsorption phase of the kinetic trace.

The choice of control assay from which to derive $\Delta\vartheta$ is important for the accuracy of the kinetic parameters and ultimately the derived concentration of the target species in solution. As can be seen in Fig. 6A, using glycine and IgG as a control spot assay produces similar kinetic traces with fitted rate constants of k_a (glycine) $= (1.4 \pm 0.2) \times 10^5\ M^{-1}\ s^{-1}$ and k_a (IgG) $= (1.6 \pm 0.2) \times 10^5\ M^{-1}\ s^{-1}$, whereas the fitted rate constant for fibrinogen is k_a (fibrinogen) $= (1.8 \pm 0.3) \times 10^5\ M^{-1}\ s^{-1}$. The isoelectric points for glycine, fibrinogen, and IgG are *p*I (glycine) = 5.97, *p*I (fibrinogen) = 5.8, and *p*I (IgG) = 6.0 [26], suggesting that all three surfaces are negatively charged at physiological pH and that the interaction is not purely electrostatic but rather there are some additional protein–protein interactions that determine the measurements in the whole serum. The faster rate and lower ϑ_m for fibrinogen, together with the similar rates observed for glycine and IgG surfaces, suggest that nonspecific binding observed for the fibrinogen spots is a misnomer for these processes, and the kinetics is indicative of the specific fibrinogen protein–protein interactions with the antiserum proteins.

The antibody–antigen interaction is controlled by two rate constants: the adsorption rate k_a and the desorption rate k_d (Eq. (4)). Each of the kinetic traces at the different aBSA concentrations can be analyzed in detail. The data set collected at different con-

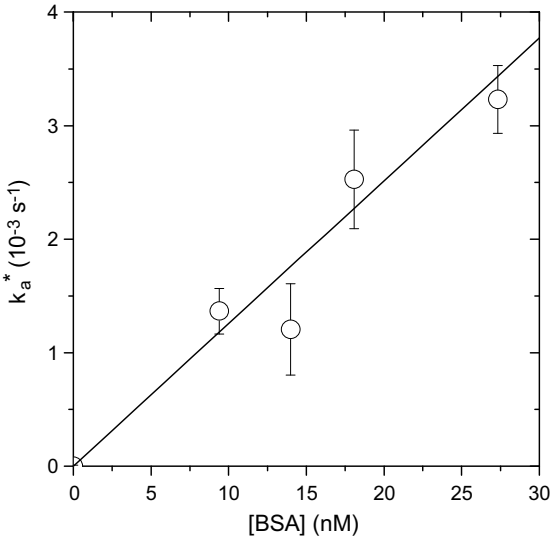

Fig. 8. Pseudo-first-order rate constants for BSA antibody–antigen binding derived from light scattering array sensor data. The slope from the linear fit corresponds to the second-order rate constant $k_a = (1.3 \pm 0.3) \times 10^5\ M^{-1}\ s^{-1}$.

centrations of analyte (0–30 nM aBSA) shows the expected variation of rates with increasing concentrations (Fig. 6B), and a plot of the observed pseudo-first-order rate constant versus concentration shows a linear plot from which the second-order rate constant, $k_a = (1.3 \pm 0.3) \times 10^5\ M^{-1}\ s^{-1}$, may be derived (Fig. 8). Switching the buffer back to PBS, however, causes the aBSA–BSA complex to dissociate, and k_d may then be determined from the desorption phase (Fig. 7) and averaged over the data set. The two rate constants are $k_a = (1.4 \pm 0.2) \times 10^5\ M^{-1}\ s^{-1}$ and $k_d = (4 \pm 2) \times 10^{-4}\ s^{-1}$, from which $K_D = k_d/k_a = 3 \pm 2$ nM. Taking the parameters obtained from the linear pseudo-first-order plot (Fig. 8), we may derive the concentration of the antibody in the antiserum from the single-trace data (Fig. 7) as 8.8 ± 2.0 nM. This may be compared with the stated concentration (based on the manufacturer specification) of 9.5 nM, an error of 15%, which represents the future accuracy of the array reader at determining the antibody concentration in antiserum.

The same measurements were performed on the SensiQ continuous gold SPR platform in our laboratory and by Nomadics [27], and from these values of K_D also were derived (Table 2). There have been other reports of aBSA–BSA kinetics in the literature [27–29], including a study where the coupling was used to attach red blood cells to the surface [30]. In that study, the k_a rate constant was diffusion limited by the red blood cells onto which the antigen was attached. Similarly, a recent study on Biacore instruments in 22 laboratories determined the association and dissociation rate constants for prostate-specific antigen (PSA) and its antibody. The rate constants $k_a = (4.1 \pm 0.6) \times 10^4\ M^{-1}\ s^{-1}$ and $k_d = (4.5 \pm 0.6) \times 10^{-5}\ s^{-1}$ [31], leading to a $K_D = 1.1 \pm 0.2$ nM. The deviation in the measurements across the laboratories is 15% (1 SD). Furthermore, an analysis of myoglobin-anti-myoglobin gave $k_a = 2.6 \times 10^4\ M^{-1}\ s^{-1}$ and $k_d = 2.0 \times 10^{-3}\ s^{-1}$ [32], indicating that the measurements on the SensiQ and array reader platforms are consistent with antibody–antigen binding events reported across the literature.

The scattering intensity change at the nanoparticle surface may be calibrated using the change in *RI* of bulk solutions of known compositions, from which the maximum change in *RI* for aBSA–BSA may be determined as $(5.6 \pm 0.1) \times 10^{-3}$ RIU. This figure may be compared with the change in *RI* observed on the continuous gold platform of $(9.5 \pm 0.1) \times 10^{-4}$ RIU, resulting in a particle/surface $\triangle RI_{bulk}$ ratio of 5.9. Studies on continuous gold surfaces have derived a conversion of 10^{-3} RIU = 1 ng mm^{-2} [27,33–36], so that from our value of $\vartheta_m = 5.6 \times 10^{-3}$ RIU we obtain 5.6 ng mm^{-2} or 1.6 to 2.1 layers of IgG on the surface.

The interaction between the plasmon field and the biologically active layer is the important factor in controlling the sensitivity of the plasmon to the binding event. To a first approximation, the plasmon field of the nanoparticle penetrates approximately 60 nm into the medium above the nanoparticles, which may be compared with 300 nm for the continuous gold surface [37]. However, the biological layer is only approximately 10 nm thick (serum albumin has a mass of 66 kDa and the dimensions 7.5 × 7.5 × 4 nm [38], and IgG is 5 × 13 × 13 nm [39]) to allow the antigen on the surface and the antibody attachment, enabling us to define an *RI* contrast, κ, as the ratio of the integral depth of the biological layer to the exponentially decaying penetration depth of the plasmon field. For the gold nanoparticles (subscript p) or continuous surface (subscript s), the *RI* contrast ratio $\kappa_{p/s}$ is given by

$$\kappa_{p/s} = 1 - e^{-l_b/d_{p/s}}, \tag{5}$$

where $l_b = 10$ nm is the protein layer thickness and $d_{p/s}$ is the penetration depth of the respective plasmon field. An analysis of the plasmon penetration depth $d_{p/s}$ (or particle radius) versus κ_p/κ_s (the ratio of the *RI* contrast for the particle and the surface) shows that for the particles we have been using in the experiment the ratio is 4.68, in excellent agreement with the greater sensitivity of the nanoparticles to the aBSA–BSA layer. This may point to a general advantage that particles have over continuous surfaces that have a large penetration depth and, thus, are sensitive to changes in the bulk *RI* well above the biologically active surface that is a source of *RI* noise and poor *RI* contrast.

Table 2
Specific BSA antibody–antigen interaction rate constants from the array reader and SensiQ plasmon platforms.

	k_a ($10^5\ M^{-1}\ s^{-1}$)	k_d ($10^{-4}\ s^{-1}$)	K_D (nM)
Array reader (aBSA)–(glycine)	1.3 ± 0.2	4 ± 2	3 ± 2
Array reader (aBSA)–(IgG)	1.6 ± 0.2		
Array reader (aBSA)–(fibrinogen)	1.8 ± 0.3		
SensiQ	1.7 ± 0.2	3 ± 2	2 ± 2
SensiQ (Nomadics aBSA immobilized)	1.46	3.52	2.4 ± 0.1

Note: Values are means ± 2 SD.

Conclusion

An array, printed with seed nanoparticles and grown into larger particles by surface synthesis, has been functionalized with proteins and used successfully to screen for antibodies in whole blood sera. The label-free detection platform was interrogated using a simple array reader that monitors the change in scattered light intensity from the surface nanoparticles on binding the target antibody. The detection limit is 10^{-8} M, corresponding to an antibody concentration in a serum of 1 μg ml^{-1}. Comparison of the sensitivity of the nanoparticle surface with that of the continuous gold surface indicates a fivefold greater sensitivity of the particles when interpreted in terms of the *RI* contrast of the biologically active layer to bulk within the plasmon field. The *RI* contrast advantage suggests that particles may be engineered to a specific length and aspect ratio to optimize the scattering efficiency and maximize the *RI* contrast advantage for a specific biological assay.

Acknowledgment

The work was supported by Research Councils UK (RCUK, Basic Technology Grant, EP/C52389X/1).

References

[1] S.R. Weinberger, E.A. Dalmasso, E.T. Fung, Current achievements using ProteinChip Array technology, Curr. Opin. Chem. Biol. 6 (2002) 86–91.
[2] A. Sreekumar, M.K. Nyati, S. Varambally, T.R. Barrette, D. Ghosh, T.S. Lawrence, A.M. Chinnaiyan, Profiling of cancer cells using protein microarrays: discovery of novel radiation-regulated proteins, Cancer Res. 61 (2001) 7585–7593.
[3] H. Caron, B. van Schaik, M. van der Mee, F. Baas, G. Riggins, P. van Sluis, M.-C. Hermus, R. van Asperen, K. Boon, P.A. Voute, S. Heisterkamp, A. van Kampen, R. Versteeg, The human transcriptome map: clustering of highly expressed genes in chromosomal domains, Science 291 (2001) 1289–1292.
[4] G. MacBeath, Protein microarrays and proteomics, Nat. Genet. 32 (2002) 526–532.
[5] A. Haes, R. Duyne, A unified view of propagating and localized surface plasmon resonance biosensors, Anal. Bioanal. Chem. 379 (2004) 920–930.
[6] R.L. Rich, D.G. Myszka, Survey of the year 2005 commercial optical biosensor literature, J. Mol. Recogn. 19 (2006) 478–534.
[7] R.L. Rich, D.G. Myszka, Higher-throughput, label-free, real-time molecular interaction analysis, Anal. Biochem. 361 (2007) 1–6.
[8] D. Wassaf, G. Kuang, K. Kopacz, Q.-L. Wu, Q. Nguyen, M. Toews, J. Cosic, J. Jacques, S. Wiltshire, J. Lambert, C.C. Pazmany, S. Hogan, R.C. Ladner, A.E. Nixon, D.J. Sexton, High-throughput affinity ranking of antibodies using surface plasmon resonance microarrays, Anal. Biochem. 351 (2006) 241.
[9] B. Rick, J.C. Gregory, C. Anthony, P. Michelle, J.S. Lawrence, E.A. Jaime, Induced fit of an epitope peptide to a monoclonal antibody probed with a novel parallel surface plasmon resonance assay, J. Biol. Chem. 280 (2005) 4188.
[10] J. Yuk, D.-G. Hong, J.-W. Jung, S.-H. Jung, H.-S. Kim, J.-A. Han, Y.-M. Kim, K.-S. Ha, Sensitivity enhancement of spectral surface plasmon resonance biosensors for the analysis of protein arrays, Eur. Biophys. J. 35 (2006) 469–476.

[11] A. Haes, D. Stuart, S. Nie, R. Van Duyne, Using solution-phase nanoparticles, surface-confined nanoparticle arrays, and single nanoparticles as biological sensing platforms, J. Fluoresc. 14 (2004) 355–367.
[12] S. Wang, D.F.P. Pile, C. Sun, X. Zhang, Nanopin plasmonic resonator array and its optical properties, Nano Lett. 7 (2007) 1076–1080.
[13] L.S. Jung, C.T. Campbell, T.M. Chinowsky, M.N. Mar, S.S. Yee, Quantitative interpretation of the response of surface plasmon resonance sensors to adsorbed films, Langmuir 14 (1998) 5636–5648.
[14] T. Jensen, L. Kelly, A. Lazarides, G.C. Schatz, Electrodynamics of noble metal nanoparticles and nanoparticle clusters, J. Cluster Sci. 10 (1999) 295–317.
[15] A.J. Haes, R.P. Van Duyne, A nanoscale optical biosensor: Sensitivity and selectivity of an approach based on the localized surface plasmon resonance spectroscopy of triangular silver nanoparticles, J. Am. Chem. Soc. 124 (2002) 10596–10604.
[16] R.G. Osifchin, R.P. Andres, J.I. Henderson, C.P. Kubiak, R.N. Dominey, Synthesis of nanoscale arrays of coupled metal dots, Nanotechnology 7 (1996) 412–416.
[17] N. Félidj, J. Aubard, G. Lévi, J.R. Krenn, M. Salerno, G. Schider, B. Lamprecht, A. Leitner, F.R. Aussenegg, Controlling the optical response of regular arrays of gold particles for surface-enhanced Raman scattering, Phys. Rev. B 65 (2002) 075419.
[18] G. Zeder-Lutz, E. Zuber, J. Witz, M.H.V. Van Regenmortel, Thermodynamic analysis of antigen–antibody binding using biosensor measurements at different temperatures, Anal. Biochem. 246 (1997) 123–132.
[19] P.R. Edwards, R.J. Leatherbarrow, Determination of association rate constants by an optical biosensor using initial rate analysis, Anal. Biochem. 246 (1997) 1–6.
[20] R.V. Olkhov, A.M. Shaw, Label-free antibody–antigen binding detection by optical sensor array based on surface-synthesized gold nanoparticles, Biosens. Bioelectron. 23 (2008) 1298–1302.
[21] G.T. Hermanson, A.K. Mallia, P.K. Smith, Immobilized Affinity Ligand Techniques, Academic Press, San Diego, 1992.
[22] C.J. Murphy, T.K. Sau, A.M. Gole, C.J. Orendorff, J. Gao, L. Gou, S.E. Hunyadi, T. Li, Anisotropic metal nanoparticles: Synthesis, assembly, and optical properties, J. Phys. Chem. B 109 (2005) 13857–13870.
[23] N.R. Jana, L. Gearheart, C.J. Murphy, Wet chemical synthesis of high aspect ratio cylindrical gold nanorods, J. Phys. Chem. B 105 (2001) 4065–4067.
[24] K-Y. Chu, A.R. Thompson, Densities and refractive indices of alcohol–water solutions of *n*-propyl, isopropyl, and methyl alcohols, J. Chem. Eng. Data 7 (1962) 358–360.
[25] C. Noguez, Surface plasmons on metal nanoparticles: The influence of shape and physical environment, J. Phys. Chem. C 111 (2007) 3806–3819.
[26] D. Malamud, J.W. Drysdale, Isoelectric points of proteins: A table, Anal. Biochem. 86 (1978) 620–647.
[27] J. Quinn, A. Martin, J. Harvard, Kinetic Analysis of Protein–Protein Interactions, Nomadics, Oklahoma City, OK, 2007.
[28] A.W. Sonesson, T.H. Callisen, H. Brismar, U.M. Elofsson, A comparison between dual polarization interferometry (DPI) and surface plasmon resonance (SPR) for protein adsorption studies, Colloids Surf. B 54 (2007) 236–240.
[29] A. Leung, P.M. Shankar, R. Mutharasan, Real-time monitoring of bovine serum albumin at femtogram/mL levels on antibody-immobilized tapered fibers, Sens. Actuat. B 123 (2007) 888–895.
[30] B. Li, J. Chen, M. Long, Measuring binding kinetics of surface-bound molecules using the surface plasmon resonance technique, Anal. Biochem. 377 (2008) 195–201.
[31] P.S. Katsamba, I. Navratilova, M. Calderon-Cacia, L. Fan, K. Thornton, M. Zhu, T.V. Bos, C. Forte, D. Friend, I. Laird-Offringa, G. Tavares, J. Whatley, E. Shi, A. Widom, K.C. Lindquist, S. Klakamp, A. Drake, D. Bohmann, M. Roell, L. Rose, J. Dorocke, B. Roth, B. Luginbühl, D.G. Myszka, Kinetic analysis of a high-affinity antibody/antigen interaction performed by multiple Biacore users, Anal. Biochem. 352 (2006) 208–221.
[32] R. Karlsson, A. Falt, Experimental design for kinetic analysis of protein–protein interactions with surface plasmon resonance biosensors, J. Immunol. Methods 200 (1997) 121–133.
[33] J.B.F.A.V.J.A. De Feijter, Ellipsometry as a tool to study the adsorption behavior of synthetic and biopolymers at the air–water interface, Biopolymers 17 (1978) 1759–1772.
[34] B.A. Snopok, K.V. Kostyukevych, O.V. Rengevych, Y.M. Shirshov, E.F. Venger, A biosensor approach to probe the structure and function of the adsorbed proteins: fibrinogen at the gold surface, Semicond. Phys. Quantum Electron. Optoelectron. 1 (1998) 121–134.
[35] M.S. Yuri, I.C. Vladimir, V.S. Yuri, E.P. Matsas, A.E. Rachcov, T.A. Sergeeva, Determination of polarizability and surface concentration of biomolecules using surface plasmon resonance experiment. in: V.S. Sergey, Y.V. Mikhail (Eds.), Proceedings of SPIE, 1995, pp. 118–123.
[36] P.A. Cuypers, J.W. Corsel, M.P. Janssen, J.M. Kop, W.T. Hermens, H.C. Hemker, The adsorption of prothrombin to phosphatidylserine multilayers quantitated by ellipsometry, J. Biol. Chem. 258 (1983) 2426–2431.
[37] C.R. Yonzon, E. Jeoung, S. Zou, G.C. Schatz, M. Mrksich, R.P. Van Duyne, A comparative analysis of localized and propagating surface plasmon resonance sensors: the binding of concanavalin A to a monosaccharide functionalized self-assembled monolayer, J. Am. Chem. Soc. 126 (2004) 12669–12676.
[38] S. Sugio, A. Kashima, S. Mochizuki, M. Noda, K. Kobayashi, Crystal structure of human serum albumin at 2.5 Å resolution, Protein Eng. 12 (1999) 439–446.
[39] L.J. Harris, S.B. Larson, K.W. Hasel, A. McPherson, Refined structure of an intact IgG_{2a} monoclonal antibody, Biochemistry 36 (1997) 1581–1597.